J. Sens. Sens. Syst., 6, 1–8, 2017
www.j-sens-sens-syst.net/6/1/2017/
doi:10.5194/jsss-6-1-2017

JSSS
Journal of Sensors and Sensor Systems
Open Access

A mode-localized MEMS electrical potential sensor based on three electrically coupled resonators

Chun Zhao[1], **Graham S. Wood**[1], **Suan Hui Pu**[1,2], **and Michael Kraft**[3]

[1]Nano Research Group, School of Electronics and Computer Science, University of Southampton,
Southampton, SO17 1BJ, UK
[2]University of Southampton Malaysia Campus, Nusajaya, 79200 Johor, Malaysia
[3]Montefiore Institute, University of Liège, Liège, Belgium

Correspondence to: Michael Kraft (m.kraft@ulg.ac.be)

Received: 20 September 2016 – Revised: 2 December 2016 – Accepted: 6 December 2016 – Published: 9 January 2017

Abstract. We report a new class of MEMS resonant potential sensor based on the mode localization effect using a 3-degree-of-freedom (DoF) electrically weakly coupled resonator system. As opposed to previously reported electrically coupled 2DoF mode-localized resonant sensors, it can be shown in theory that the 3DoF structure has an improved sensitivity without sacrificing signal transduction, in addition to a reduced nonideal effect with regard to the vibration amplitudes and the motional currents. Experimentally, it has also been shown that several orders of magnitude higher sensitivity can be achieved compared to frequency shift and 2DoF mode-localized sensor. In the best case, we are able to demonstrate over 4 orders of magnitude improvement in sensitivity compared to frequency shift as an output signal. Compared to current state-of-the art 2DoF mode-localized sensor, the highest sensitivity improvement is over 123 times. An estimation of the noise floor of the sensor is $614\,\mu\mathrm{V}/\sqrt{\mathrm{Hz}}$ for potential sensing, or an equivalent $57.6e/\sqrt{\mathrm{Hz}}$ for charge sensing, and a dynamic range of 66.3 dB can be achieved. Furthermore, two different approaches for detection were investigated, perturbing the stiffness in the form of either an axial electrostatic force or a change in electrostatic spring. We were able to demonstrate that the approach of changing electrostatic spring is more sensitive than its counterpart.

1 Introduction

The detection of electrical potential is of significant interest in surface potential distribution characterizations (Nonnenmacher et al., 1991) and biological (Sinensky and Belcher, 2007) and chemical analysis (Gao and Cai, 2009). Electrometers (Lee et al., 2008) are another application for potential sensing devices, which can be employed for particulate matter detection (Jaramillo et al., 2013). MEMS resonant devices have been widely used for these applications with the advantage of high resolution and a large dynamic range.

Recently, mode-localized MEMS resonant sensors have emerged as an alternative resonant sensing scheme (Thiruvenkatanathan et al., 2009; Zhao et al., 2015b), in which the mode shape of a weakly coupled resonator system changes subject to an external stiffness perturbation caused by the electrical potential change. Orders of magnitude improvement in sensitivity for electrometers (Thiruvenkatanathan et al., 2010a; Zhang et al., 2016a) have already been reported. Furthermore, mode-localized sensors exhibit better common-mode rejection capability (Thiruvenkatanathan et al., 2010b). Previously, mode-localized sensors were implemented with two resonators weakly coupled electrically (Thiruvenkatanathan et al., 2011) or mechanically (Spletzer et al., 2006; Zhang et al., 2016b), with the electrical coupling element offering advantages of tunability of the sensitivity (Manav et al., 2014).

In this paper, we demonstrate an alternative approach for potential sensing applications using a 3-degree-of-freedom (3DoF) structure. The structure has already been reported elsewhere (Zhao et al., 2016); however, the advantages of the 3DoF design have not been discussed in full detail, as only improvements in sensitivity have been shown. In this paper, we focus on the design considerations of the 3DoF structure, which we believe also have other advantages – for instance,

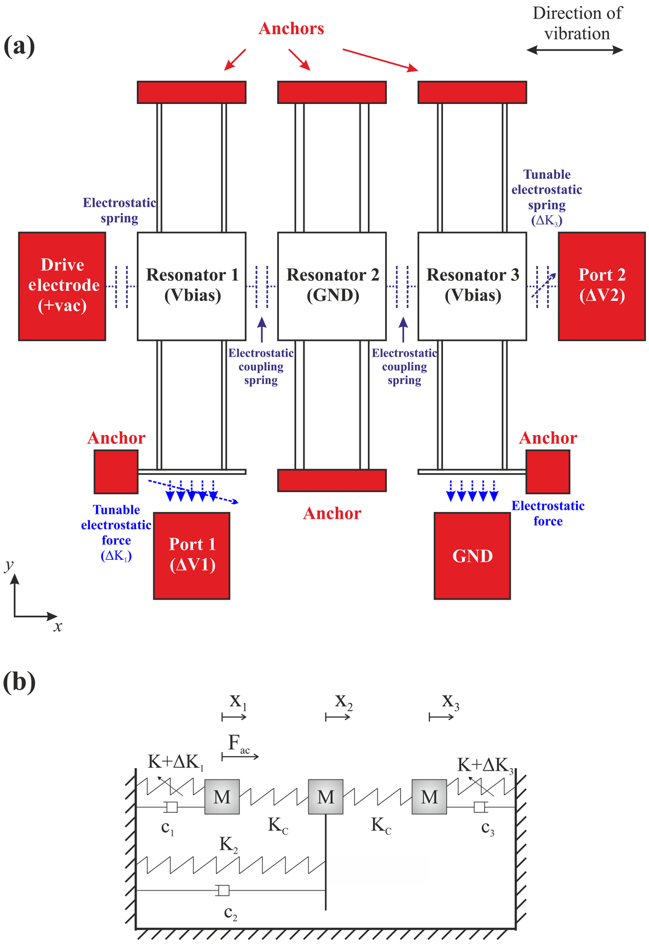

Figure 1. **(a)** Schematics of the 3DoF mode-localized potential sensor, showing three resonators coupled electrostatically with their neighbours. In addition, electrostatic springs and forces caused by electrical potential differences are also shown; **(b)** the linearized spring–mass–damper model of the 3DoF mode-localized potential sensor.

the alleviation of the electrical nonlinear driving force, as well as the nonideal sensing current. Furthermore, in terms of potential sensing applications, two sensing methods exist: (i) modulating the electrostatic spring and (ii) directly applying an axial electrostatic force. However, the two sensing methods were not directly compared previously. In this work, we are able to demonstrate that, by modulating the electrostatic spring, an improvement in sensitivity can be observed.

The paper is arranged as follows: in Sect. 2, the advantages of the 3DoF structure design are discussed; in Sect. 3, the two potential sensing schemes by applying a DC potential to different ports are discussed; in Sect. 4, experimental results are presented and the paper is concluded in Sect. 5.

2 Advantages of the 3DoF structure with electrical coupling

The schematic of the 3DoF mode-localized MEMS resonant potential sensor is shown in Fig. 1. Each resonator has four suspension beams acting as springs and a relatively large proof mass to reduce the effect of fabrication tolerances to the mass. In addition, resonators 1 and 3 have a tether structure that is capable of translating an axial electrostatic force to the suspension beams. Electrical coupling was chosen due to the ability to tune the coupling strength and thus the sensitivity of the sensor to external perturbations. A DC voltage V_{bias} was applied to resonators 1 and 3, while resonator 2 was connected to ground. The voltage difference created electrostatic springs to couple the resonators to its neighbouring counterparts. An AC drive voltage is applied on the drive electrode, generating the actuation force. Details of the design and its fabrication process were reported in Zhao et al. (2016). However, due to the limited scope of the previous work, the advantages of the design were not discussed in full detail; these are presented in the following sections.

2.1 Sensitivity improvement

As reported in Zhao et al. (2015b), the sensitivity to stiffness changes of a 3DoF mode-localized resonant sensor can be expressed by, assuming linear springs, $K_2 > 2K$ and $K/K_c > 10$:

$$\mathcal{S}_{\text{3DoF}} = \left| \frac{\partial(\text{Amplitude ratio})}{\partial(\Delta K/K)} \right| = \frac{K(K_2 - K + K_c)}{K_c^2}, \tag{1}$$

where K, K_2 and K_c denote the stiffness of the suspension beam of resonator 1 (and 3), resonator 2 and the coupling spring, respectively. Moreover, the sensitivity of a 2DoF mode-localized resonant sensor can be expressed by Thiruvenkatanathan (2010):

$$\mathcal{S}_{\text{2DoF}} = \left| \frac{\partial(\text{Amplitude ratio})}{\partial(\Delta K/K)} \right| = \left| \frac{K}{2K_c} \right|. \tag{2}$$

For identical K/K_c, the sensitivity of the 3DoF mode-localized resonant sensor can be enhanced by a factor of $\frac{K_2 - K + K_c}{K_c}$. Over 2 orders of magnitude improvement has already been demonstrated (Zhao et al., 2016).

2.2 Sensitivity improvement without sacrificing signal transduction

The electrostatic coupling K_c for a parallel plate configuration as shown in Fig. 1 can be expressed by Thiruvenkatanathan (2010):

$$K_c = -\frac{\varepsilon_0 A V^2}{d^3}, \tag{3}$$

where ε_0, A and d are the dielectric constant of vacuum, cross-sectional area and the air gap between the plates, respectively. V is the potential difference between the two plates, which is the determining factor of the coupling strength for a given design. Therefore, for a 2DoF mode-localized resonant sensor, decreasing V, and thus K_c, is beneficial for sensitivity enhancement. On the other hand, a high V is often desirable due to the required motional current level for a reasonable signal-to-noise ratio in the readout circuit.

This design contradiction for choosing an optimal V can be solved by adopting a 3DoF resonant sensor configuration. An additional third parameter, the effective spring constant of the middle resonator K_2, can be altered to maintain or even improve the sensitivity without sacrificing the readout signal level. As shown in Eq. (1), increasing K_2 can improve the sensitivity.

2.3 Electrostatic nonlinearity reduction

For an ideal 3DoF mode-localized resonant sensor with identical resonators 1 and 3 and negligible damping, there are three fundamental modes of vibration (Nguyen, 1999): in the first mode, all three resonators vibrate in phase with each other; in the second mode, resonators 1 and 3 vibrate out of phase, whereas resonator 2 is statutory; in the third mode, each resonator vibrates out of phase with its neighbours, and resonators 1 and 3 are in phase. The second mode, which is referred to as out-of-phase mode, is the focus of this study. The balanced and perturbed mode shapes of the out-of-phase mode of a 3DoF resonant structure are illustrated in Fig. 2.

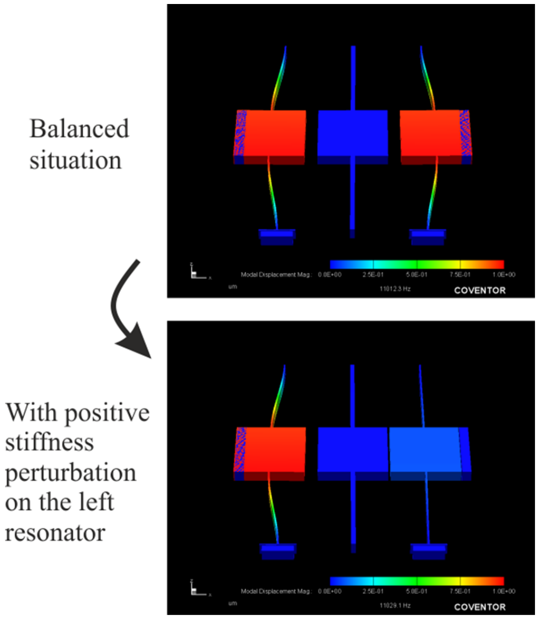

Figure 2. Illustration of the mode shapes of the out-of-phase mode of a representative 3DoF resonant structure, simulated using CoventorWare FEM tool: (top) without perturbations and (bottom) with stiffness perturbations. The perturbation in the bottom panel is a positive stiffness perturbation applied to resonator 1. It should be pointed out that the same mode shape is generated given an identical negative stiffness perturbation applied to resonator 3.

When a stiffness perturbation is introduced, resonator 2 starts to vibrate due to mode localization. However, in the case of weak coupling, the amplitude of resonator 2 is orders of magnitude lower than the resonator with highest amplitude (e.g. resonator 1) (Zhao et al., 2015a). This can also be seen qualitatively from Fig. 2.

Consider an abstract model of the drive electrode, resonator 1 and resonator 2 as shown in Fig. 3. Only resonator 1 is considered because, under normal operating conditions, resonator 1 has a higher amplitude than resonator 3, meaning that it is more susceptible to nonlinear effects, as will be shown in Sect. 4.

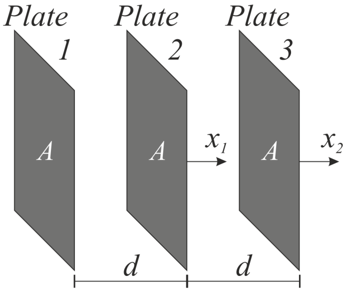

Figure 3. Abstract model of the drive electrode, resonator 1 and resonator 2 illustrated as parallel plates. X_1 and X_2 are the displacement of resonator 1 and resonator 2, respectively. The cross-sectional area A and gap d are supposed to be identical for all electrodes considered.

Assuming $v_{\mathrm{ac}} \ll V_{\mathrm{bias}}$ and neglecting nonlinear terms with orders higher than 3, the total electrostatic force exerted on resonator 1 can be approximated by

$$\begin{aligned} F_{\mathrm{total,elec}} \approx{}& \eta_{A,P} v_{\mathrm{ac}} \sin\omega t + \frac{\varepsilon_0 V_{\mathrm{bias}}^2 A}{d^3} X_1 \\ &+ \frac{\varepsilon_0 V_{\mathrm{bias}}^2 A}{d^3}(X_1 - X_2) \\ &- \frac{3\varepsilon_0 V_{\mathrm{bias}}^2 A}{2d^4}\left[X_1^2 - (X_1 - X_2)^2\right] \\ &+ \frac{2\varepsilon_0 V_{\mathrm{bias}}^2 A}{d^5}\left[X_1^3 + (X_1 - X_2)^3\right]. \end{aligned} \tag{4}$$

For a 3DoF mode-localized sensor with $X_2 \ll X_1$, or *quasi-static* motion of resonator 2, the second-order nonlinear term of the electrostatic actuation (i.e. between drive electrode and resonator 1) cancels out that of the electrostatic coupling (i.e. between resonators 1 and 2), therefore rendering the total second-order electrostatic nonlinearity negligible. Thus the overall nonlinearity is reduced. This is often desirable for resonator design, leaving only the third-order electrostatic nonlinearity which, in turn, can be used to eliminate the third-order mechanical nonlinearity intrinsic to the vibrating beams (Shao et al., 2008).

As for a 2DoF mode-localized sensor with comparable X_1 and X_2, the second-order nonlinear terms remains; thus

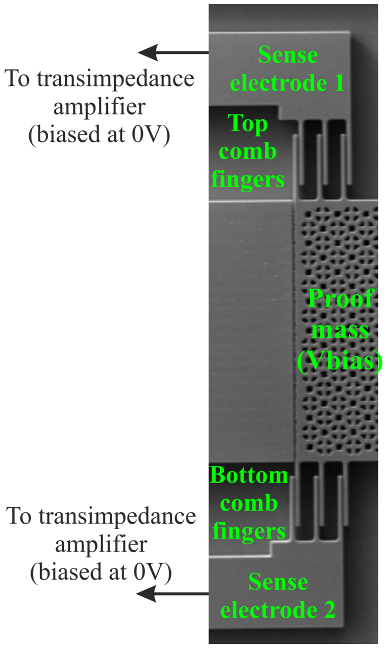

Figure 4. An SEM image of one pair of comb fingers attached to the proof mass of resonator 1 for vibration motion sensing. (As shown in Fig. 5c, another pair of comb fingers with identical configuration is also attached to the proof mass of resonator 3.) The top and bottom sets of the comb fingers on the proof mass are reversely configured relative to the stationary sense electrodes 1 and 2; this enables differential sensing. Therefore, a reduction in nonideal sense current components is achieved by common-mode rejection.

the total nonlinearity is higher than that of a 3DoF mode-localized resonant sensor.

2.4 Reduction of nonideal sense current components

Due to the amplitude detecting method used in a mode-localized sensor, it is important to obtain a measure of the linear motion of the resonators with high accuracy. From the structure design perspective, it is desirable to use differential sensing to cancel out the common-mode second-order nonlinearity while doubling the magnitude of the first-order term. This is shown in Fig. 4. In addition to the second-order nonlinear term of the motional current, another common-mode nonideal current component, the feed-through current (Lee and Seshia, 2009), can also be cancelled out.

3 Potential sensing methods

Using two different approaches, we investigated the application of the device to detect a DC electrical potential applied to either "port 1" or "port 2", as illustrated in Fig. 1a. When a DC potential is applied to port 1, an axial electrostatic force change is created, modulating the stress in the suspension beams and thus leading to a stiffness perturbation of resonator 1. Alternatively, when a DC potential is applied to port 2, a change in the electrostatic spring, instead of an electrostatic force, modulates the spring softening effect compared to the case in which no potential is applied; this is equivalent to introducing a stiffness perturbation to resonator 3.

3.1 Potential detection using port 1

The stiffness perturbation of resonator 1, ΔK_1, as a function of an applied potential V_1 to port 1, can be expressed as (Zhao et al., 2015b)

$$\Delta K_1 = \frac{1.2\varepsilon_0 A_1(-2V_{\mathrm{bias}}V_1 + V_1^2)}{d_1^2 L}, \tag{5}$$

where ε_0 is the dielectric constant of free space. Typically, to initially avoid mode aliasing, a negative stiffness perturbation, $K_{\mathrm{p}} < 0$, created by a constant voltage V_{p} on port 2 is introduced (Zhao et al., 2015b). With an applied K_{p}, the sensing mechanism in response to a stiffness perturbation caused by the potential change is explained below. Assuming $|\Delta K_1| \ll |K_{\mathrm{p}}|$, based on a transfer function model of the 3DoF weakly coupled resonators device described in Zhao et al. (2015b), the mode frequencies of interest can be calculated as

$$\omega \approx \sqrt{\frac{K' + K_{\mathrm{c}} + \frac{1}{2}\left(\Delta K' - \frac{2K'}{\gamma} \pm \sqrt{\Delta K'^2 + \left(\frac{2K'}{\gamma}\right)^2}\right)}{M}}, \tag{6}$$

where $K' = K + \Delta K_1$, $\Delta K' = \Delta K_1 - K_{\mathrm{p}}$, $\gamma = \frac{K(K_2 - K + K_{\mathrm{c}})}{K_{\mathrm{c}}^2}$, M is the effective mass of each of all three resonators, K is the stiffness of resonators 1 and 3, K_2 is the stiffness of resonator 2 and $K_{\mathrm{c}} = -\frac{\varepsilon_0 A V_{\mathrm{bias}}^2}{d^3}$ is the electrostatic coupling stiffness between neighbouring resonators. The positive and negative sign is for the out-of-phase and in-phase mode, respectively.

From Eq. (6), it can be derived that the out-of-phase mode has a more significant response subject to a stiffness perturbation. Also, assuming $V_1 \ll V_{\mathrm{bias}}$ and weak coupling, $K_{\mathrm{c}} \ll K$, we can find an expression of the sensitivity for frequency shift as an output signal, $\mathcal{S}_{f,1}$, with respect to V_1:

$$\mathcal{S}_{f,1} = \frac{\partial\left(\left|\frac{\Delta f}{f}\right|\right)}{\partial(\Delta K)}\frac{\partial(\Delta K)}{\partial(V_1)} \approx -\frac{1.2\varepsilon_0 A_1 V_{\mathrm{bias}}}{d_1^2 L K}. \tag{7}$$

It can be seen that Eq. (7) is similar to a conventional single DoF resonant sensor with frequency shift as an output signal (Schmidt and Howe, 1987), allowing a direct comparison to using amplitude ratio as an output signal.

If a mode-localized sensing approach is used, the linearized sensitivity of amplitude ratio as an output with respect to the potential, $\mathcal{S}_{\mathrm{AR}}$, can be calculated based on the assumption of weak coupling as elaborated in Zhao et al. (2016), and $V_1 \ll V_{\text{bias}}$:

$$\mathcal{S}_{\text{AR},1} = \frac{\partial\left(\left|\frac{X_1(j\omega_{\text{op}})}{X_3(j\omega_{\text{op}})}\right|\right)}{\partial(\Delta K)} \frac{\partial(\Delta K)}{\partial(V_1)} \approx -\frac{2.4A_1(K_2-K+K_\text{c})d^4}{\varepsilon_0 L A^2 V_{\text{bias}}^3}, \tag{8}$$

where L is the length of the suspension beams, and A_i and d_i are the overlapping cross-sectional area and the gap of the parallel plate for the ith potential port ($i = 1$ and 2), respectively; A and d are the cross-sectional area and the gap of the electrodes for the electrostatic coupling, respectively.

It can be seen that the improvement in sensitivity is 2γ. For weak coupling $K_\text{c} < K/10 < K_2/20$, the improvement is at least 2 orders of magnitude (Zhao et al., 2016).

3.2 Potential detection using port 2

For a potential applied to port 2, $V_2 \ll V_{\text{bias}}$, cancelling the common term to both resonators 1 and 3 proportional to V_{bias}^2, the stiffness perturbation of resonator 3 can be approximated as a linear function of V_2:

$$\Delta K_3 \approx \frac{2\varepsilon_0 A_2 V_{\text{bias}} V_2}{d_2^3}. \tag{9}$$

For $|\Delta K_3| \ll |K_\text{p}|$, the in-phase mode frequency has a stronger response (Zhao et al., 2015a). The sensitivity for the in-phase mode frequency shift, as well as the amplitude ratio as an output signal, can be approximated by

$$\mathcal{S}_{f,2} = \frac{\partial\left(\left|\frac{\Delta f}{f}\right|\right)}{\partial(\Delta K)} \frac{\partial(\Delta K)}{\partial(V_2)} \approx \frac{\varepsilon_0 A_2 V_{\text{bias}}}{d_2^2 L K} \tag{10}$$

$$\mathcal{S}_{\text{AR},2} = \frac{\partial\left(\left|\frac{X_1(j\omega_{\text{op}})}{X_3(j\omega_{\text{op}})}\right|\right)}{\partial(\Delta K)} \frac{\partial(\Delta K)}{\partial(V_2)} \approx -\frac{2A_2(K_2-K+K_\text{c})d^3}{\varepsilon_0 A^2 V_{\text{bias}}^3}. \tag{11}$$

It should be noted that the length of the suspension beams is 350 µm, while the capacitive gap is 4.5 µm. Consequently, for the dimensions of this device, ΔK_1 is around 2 orders of magnitude lower than ΔK_3. Therefore, applying the potential to port 2 should induce a more significant stiffness perturbation, hence a higher output signal.

4 Experimental results and discussion

4.1 Device description

The device was fabricated by a single-mask SOI-based process with details described in Chang et al. (2011), Xie et al. (2013) and Hao et al. (2016), which achieved a good anti-stiction capability through selective roughening on the bottom side of the device layer using the notching effect. The design of the device is elaborated elsewhere (Zhao et al., 2016). Some key parameters are $L = 350\,\mu\text{m}$, $d_1 = d_2 = d = 4.5\,\mu\text{m}$, $A_1 = 160 \times 22\,(\mu\text{m})^2$ and $A_2 = A = 360 \times 22\,(\mu\text{m})^2$. The SEM image of the fabricated device is shown in Fig. 5a, with zoom-in images showing port 1 (Fig. 5b) and port 2 (Fig. 5c). In the experiment, the input impedance is dominated by the capacitances, approximately 7fF and 15fF for port 1 and port 2, respectively.

4.2 Experimental results

4.2.1 Frequency response

The electrical characterization of the device was performed under a pressure of 20 µTorr to improve the quality factor of the resonators; a Q factor of 6221 was achieved. To set the initial operating point of the sensor so that the mode aliasing effect can be avoided (Zhao et al., 2015b), a constant DC voltage $V_\text{p} = 4.15\,\text{V}$ was applied to port 2 and maintained during the experiment. An AC signal with a peak–peak amplitude of 20 mV was used to drive the resonators into oscillation for a bias voltage of $V_{\text{bias}} = 30\,\text{V}$. The motional currents of resonators 1 and 3 were converted to voltage and further amplified using an interface electronics board and recorded on an oscilloscope. The drive frequency was swept from 14 924 to 14 934 Hz manually to obtain the frequency response curve shown in Fig. 6a.

It can be seen from the frequency response that the resonator can be regarded as working in the linear regime at the out-of-phase mode frequency. Using a transimpedance gain of 6.6 MΩ, voltage gain of $200\,\text{V}\,\text{V}^{-1}$ and transduction factor of $6.05 \times 10^{-8}\,\text{V}\,\text{F}\,\text{m}^{-1}$, the vibrational amplitude can be estimated as 115 nm.

4.2.2 Potential sensitivity characterization

AC voltages were applied to the drive electrode to actuate the 3DoF system at the desired mode frequency in the linear region for different DC bias voltages.

In the first experiment, potential port 2 was maintained at the aforementioned constant DC voltage V_p for a particular V_{bias}. We then applied varying DC potentials (both positive and negative) to port 1 and measured the averaged amplitudes of resonators 1 and 3 using an oscilloscope to calculate the amplitude ratio. The same experiment was repeated for $V_{\text{bias}} = 30$, 34.5 and 40 V. The measured amplitude ratio as a function of the potential applied is plotted in Fig. 7a. Also shown is the out-of-phase mode frequency shift, normalized to the frequency when $V_1 = 0$, as a function of a potential applied to port 1 for $V_{\text{bias}} = 30\,\text{V}$. The in-phase mode frequency shift was orders of magnitude less pronounced. Therefore it is not shown.

For the second experiment, we connected port 1 to ground, while applying a DC potential to port 2. The difference between the potential applied and the aforementioned DC voltage V_p is equivalent to the potential to be sensed. The amplitude ratio with respect to the potential to be sensed is plotted in Fig. 7b. The more significant in-phase mode frequency

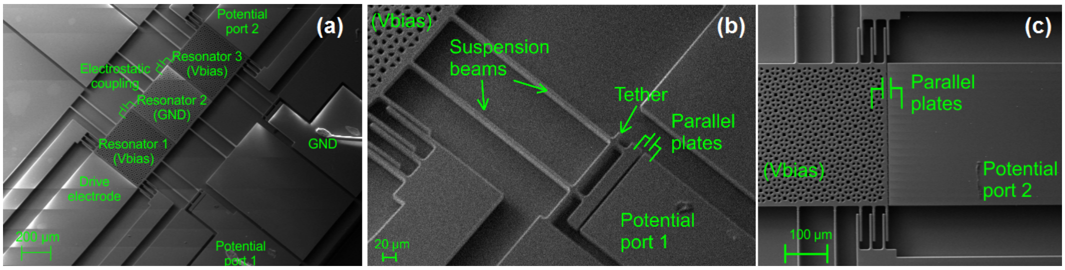

Figure 5. Scanning electron micrograph (SEM) showing **(a)** the 3DoF MEMS mode-localized resonant sensor; **(b)** the structure for potential detection at potential port 1; **(c)** the structure for potential detection at potential port 2.

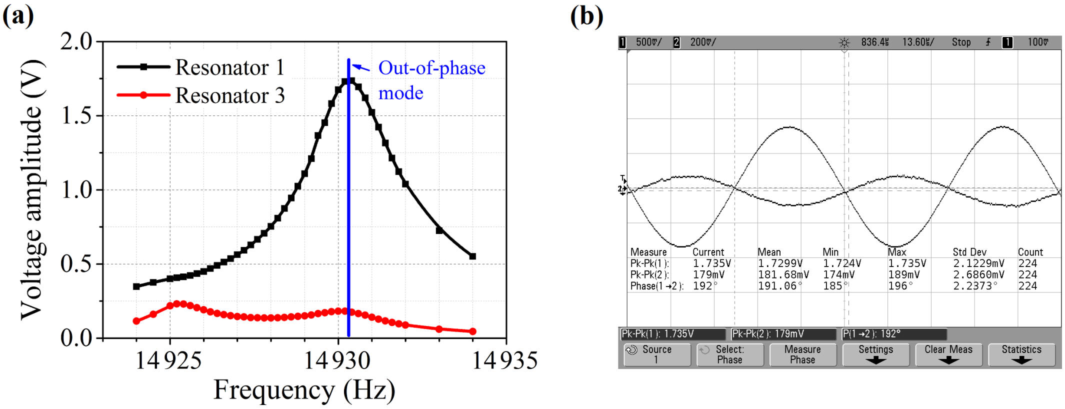

```
Measure         Current   Mean       Min      Max      Std Dev    Count
Pk-Pk(1 ):      1.735V    1.7299V    1.724V   1.735V   2.1229mV   224
Pk-Pk(2 ):      179mV     181.68mV   174mV    189mV    2.6860mV   224
Phase(1 →2 ):   192°      191.06°    185°     196°     2.2373°    224

Pk-Pk(1 ): 1.735V   Pk-Pk(2 ): 179mV   P(1 →2 ): 192°
```

Figure 6. The responses of the 3DoF mode-localized resonant sensor with a driving voltage of 20 mV and $V_{\mathrm{bias}} = 30$ V: **(a)** the frequency response of the sensor (the voltage amplitude is the peak–peak amplitude); **(b)** measured steady-state time domain responses of the resonators 1 and 3 at the out-of-phase mode frequency.

shift for $V_{\mathrm{bias}} = 30$, normalized to that of $V_2 = 0$, is also plotted in Fig. 7b.

For a potential within a range of $-5\,\mathrm{V} < V < 5\,\mathrm{V}$ (where $V \ll V_{\mathrm{bias}}$ can be considered as valid), we can extract a linear sensitivity, as given in Table 1. It can be clearly seen that when using the sensor as a mode-localized sensor, using amplitude ratio as the output signal (with sensitivity $\mathcal{S}_{\mathrm{AR}}$), there is at least 4 orders of magnitude improvement compared to frequency shift as an output (with sensitivity $\mathcal{S}_f$). This is valid for both ports 1 and 2. Comparing $\mathcal{S}_{\mathrm{AR},1}$ to $\mathcal{S}_{\mathrm{AR},2}$, it is also apparent that $\mathcal{S}_{\mathrm{AR},2}$ has over 2 orders of magnitude improvement in sensitivity for any V_{bias}. This suggests that using port 2 is superior in terms of potential sensitivity. Another observation is that the smaller V_{bias}, the higher the sensitivity. This is also predicted in theory by Eqs. (8) and (11). This will be helpful for biomedical applications where a low voltage is preferred. However, it should be pointed out that even though further reduction of the bias voltage is beneficial for the sensitivity, it also results in a reduction of full scale and thus dynamic range, due to the mode aliasing effect (Zhao et al., 2015b). For instance, when port 2 was used, the full scale was reduced from 7.3 to 4 V when V_{bias} was decreased from 40 to 30 V. Nevertheless, the maximum sensitivity improvement compared to a current state-of-the-art potential sensor (Zhang et al., 2016a), which has been employed as an electrometer having a linear sensitivity of $0.083/V$, is 123.6 times.

Using the noise estimation approach described in Zhao et al. (2015b), the noise floor of the amplitude ratio was regarded as white and derived to be $6.30 \times 10^{-3}/\sqrt{\mathrm{Hz}}$ for $V_{\mathrm{bias}} = 30$ V. For port 1, the noise floor for the potential detection is approximately $73.3\,\mathrm{mV}/\sqrt{\mathrm{Hz}}$. If port 2 is used, the performance is superior. The noise floor for the potential sensor is estimated as $614\,\mu\mathrm{V}/\sqrt{\mathrm{Hz}}$. If a measurement bandwidth of 10 Hz is assumed (after Lassagne et al., 2008), a dynamic range of 66.3 dB can be achieved. In addition, the linear fit R^2 value for $V_{\mathrm{bias}} = 30$ V for full scale is 0.999, suggesting a very linear response of the sensor. The dominant source of noise is the interface electronics (Zhao et al., 2015b), which should be optimized to improve the performance of the sensor further.

4.2.3 Equivalent charge detection

For the non-contact potential detection approach described here, the sensor can also be employed as an electrometer; the DC potential applied can be directly translated into a charge injection, with $\Delta Q = \Delta V C$ as the governing equation.

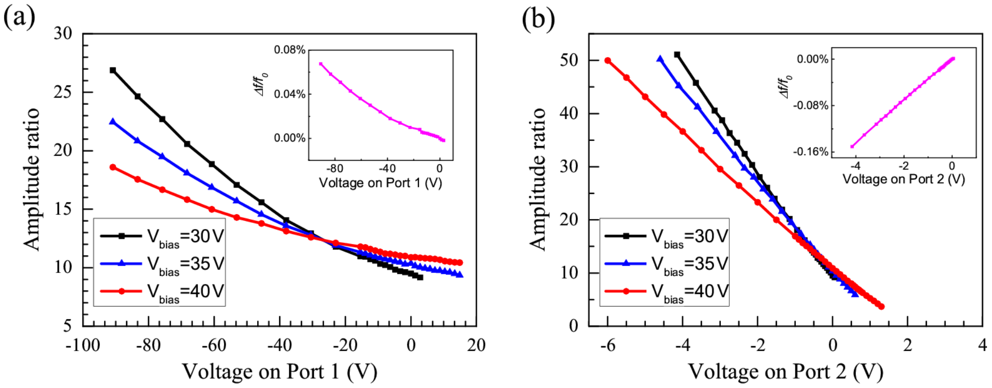

Figure 7. Graphs showing **(a)** measured amplitude ratio as a function of potential applied to port 1 for different V_{bias}, with inset showing measured normalized out-of-phase mode frequency shift for $V_{\text{bias}} = 30\,\text{V}$; **(b)** measured amplitude ratio as a function of potential applied to port 2 for different V_{bias}, with inset showing measured normalized in-phase mode frequency shift for $V_{\text{bias}} = 30\,\text{V}$.

Table 1. Summary of potential sensitivity.

Coupling	Port 1		Port 2	
voltage	$\mathcal{S}_{\text{AR},1}(/V)$	$\mathcal{S}_{f,1}(/V)$	$\mathcal{S}_{\text{AR},2}(/V)$	$\mathcal{S}_{f,2}(/V)$
30 V	−0.086	-4.28×10^{-6}	−10.26	3.57×10^{-4}
34.5 V	−0.065	NA	−8.47	NA
40 V	−0.032	NA	−6.26	NA

NA: not available.

For port 1, the motion of the resonator along the y axis direction (direction illustrated in Fig. 1) can be neglected. Therefore the parallel plate capacitance can be regarded as a constant 7fF. A resolution of $3205e/\sqrt{\text{Hz}}$ is estimated with $V_{\text{bias}} = 30\,\text{V}$.

On the other hand, due to the vibrating motion of resonator 3 along the x axis, the capacitance is not of constant value. However, due to the low vibrating amplitude (less than 12.1 nm) within the operating range for $V_{\text{bias}} = 30\,\text{V}$, the relative variation of the charge due to the motion is less than 0.27 % for a gap of 4.5 µm. If the charge variations due to the motion are neglected, the equivalent charge detection resolution is estimated to be $57.6e/\sqrt{\text{Hz}}$ with $C = 15\text{fF}$. This is an improvement of 2.5 times compared the state-of-the-art MEMS mode-localized electrometers at room temperature, which has a resolution of $147e/\sqrt{\text{Hz}}$ (Okamoto et al., 2011).

5 Conclusions

In this paper, we have demonstrated the design of a 3DoF weakly coupled resonant sensor for potential sensing applications, which could also be extended to an electrometer. We have presented the design advantages for the 3DoF structure in theory, including sensitivity improvement, electrical nonlinearity and nonideal current reduction. We have shown that, by using the device as a mode-localized sensor, the sensitivity can be improved by over 4 orders of magnitude, compared to conventional frequency shift as an output. In addition, we have also compared the sensitivity of the mode-localized sensor for different bias voltages. We demonstrated that the lower the bias voltage, the higher the sensitivity. Finally, we have shown two viable methods for sensing an electrical potential. The more sensitive approach is by applying the potential to port 2, where a change in electrostatic spring is used to perturb the stiffness. The best sensitivity improvement compared to the state-of-the-art mode-localized sensor is 123 times. If employed as an electrometer, the best resolution can also be improved by 2.5 times compared to the state of the art.

6 Data availability

The data used in this paper can be found in the Supplement.

The Supplement related to this article is available online at doi:10.5194/jsss-6-1-2017-supplement.

Edited by: R. Kirchner
Reviewed by: two anonymous referees

References

Chang, H., Xie, J., Fu, Q., Shen, Q., and Yuan, W.: Micromachined inertial measurement unit fabricated by a SOI process with selective roughening under structures, IET Micro & Nano Letters, 6, 486–489, 2011.

Gao, P. and Cai, Y.: Label-free detection of the aptamer binding on protein patterns using Kelvin probe force microscopy (KPFM), Anal. Bioanal. Chem., 394, 207–214, 2009.

Hao, Y., Xie, J., Yuan, W., and Chang, H.: Dicing-free SOI process based on wet release technology, IET Micro & Nano Letters, 11, 775–778, 2016.

Jaramillo, G., Buffa, C., Li, M., Brechtel, F. J., Langfelder, G., and Horsley, D. A.: MEMS electrometer with femtoampere resolution for aerosol particulate measurements, IEEE Sens. J., 13, 2993–3000, 2013.

Lassagne, B., Garcia-Sanchez, D., Aguasca, A., and Bachtold, A.: Ultrasensitive mass sensing with a nanotube electromechanical resonator, Nano Lett., 8, 3735–3738, 2008.

Lee, J. E.-Y., Bahreyni, B., and Seshia, A. A.: An axial strain modulated double-ended tuning fork electrometer, Sensor. Actuat. A-Phys., 148, 395–400, doi:10.1016/j.sna.2008.09.010, 2008.

Lee, J.-Y. and Seshia, A.: Parasitic feedthrough cancellation techniques for enhanced electrical characterization of electrostatic microresonators, Sensor. Actuat. A-Phys., 156, 36–42, 2009.

Manav, M., Reynen, G., Sharma, M., Cretu, E., and Phani, A.: Ultrasensitive resonant MEMS transducers with tuneable coupling, J. Micromech. Microeng., 24, 055005, doi:10.1088/0960-1317/24/5/055005, 2014.

Nguyen, C. T.: Frequency-selective MEMS for miniaturized low-power communication devices, IEEE T. Microw. Theory, 47, 1486–1503, 1999.

Nonnenmacher, M., O'Boyle, M., and Wickramasinghe, H.: Kelvin probe force microscopy, Appl. Phys. Lett., 58, 2921–2923, 1991.

Okamoto, H., Kitajima, N., Onomitsu, K., Kometani, R., Warisawa, S.-I., Ishihara, S., and Yamaguchi, H.: High-sensitivity charge detection using antisymmetric vibration in coupled micromechanical oscillators, Appl. Phys. Lett., 98, 014103, doi:10.1063/1.3541959, 2011.

Schmidt, M. A. and Howe, R. T.: Silicon Resonant Microsensors, in: 14th Automotive Materials Conference: Ceramic Engineering and Science Proceedings, 8, 1019–1034, Wiley Online Library, doi:10.1002/9780470320419.ch3, 1987.

Shao, L., Palaniapan, M., and Tan, W.: The nonlinearity cancellation phenomenon in micromechanical resonators, J. Micromech. Microeng., 18, 065014, doi:10.1088/0960-1317/18/6/065014, 2008.

Sinensky, A. K. and Belcher, A. M.: Label-free and high-resolution protein/DNA nanoarray analysis using Kelvin probe force microscopy, Nat. Nanotechnol., 2, 653–659, 2007.

Spletzer, M., Raman, A., Wu, A. Q., Xu, X., and Reifenberger, R.: Ultrasensitive mass sensing using mode localization in coupled microcantilevers, Appl. Phys. Lett., 88, 254102, doi:10.1063/1.2216889, 2006.

Thiruvenkatanathan, P.: Mode-localized sensing in micromechanical resonator arrays, PhD thesis, University of Cambridge, 2010.

Thiruvenkatanathan, P., Yan, J., Woodhouse, J., and Seshia, A.: Enhancing parametric sensitivity in electrically coupled MEMS resonators, J. Microelectromech. S., 18, 1077–1086, doi:10.1109/JMEMS.2009.2025999, 2009.

Thiruvenkatanathan, P., Yan, J., and Seshia, A.: Ultrasensitive mode-localized micromechanical electrometer, in: Frequency Control Symposium (FCS), 2010 IEEE International, 91–96, IEEE, doi:10.1109/FREQ.2010.5556368, 2010a.

Thiruvenkatanathan, P., Yan, J., and Seshia, A. A.: Differential amplification of structural perturbations in weakly coupled MEMS resonators, IEEE T. Ultrason. Ferr., 57, 690–697, doi:10.1109/TUFFC.2010.1466, 2010b.

Thiruvenkatanathan, P., Woodhouse, J., Yan, J., and Seshia, A.: Manipulating vibration energy confinement in electrically coupled microelectromechanical resonator arrays, J. Microelectromech. S., 20, 157–164, 2011.

Xie, J., Hao, Y., Shen, Q., Chang, H., and Yuan, W.: A dicing-free SOI process for MEMS devices based on the lag effect, J. Micromech. Microeng., 23, 125033, doi:10.1088/0960-1317/23/12/125033, 2013.

Zhang, H., Huang, J., Yuan, W., and Chang, H.: A High-Sensitivity Micromechanical Electrometer Based on Mode Localization of Two Degree-of-Freedom Weakly Coupled Resonators, J. Microelectromech. S., 25, 937–946, 2016a.

Zhang, H., Li, B., Yuan, W., Kraft, M., and Chang, H.: An acceleration sensing method based on the mode localization of weakly coupled resonators, J. Microelectromech. S., 25, 286–296, 2016b.

Zhao, C., Wood, G., Xie, J., Chang, H., Pu, S., and Kraft, M.: Comparative study of different output metrics for a three weakly coupled resonator sensor, in: Solid-State Sensors, Actuators and Microsystems (TRANSDUCERS), 2015 Transducers-2015 18th International Conference on, 2196–2199, IEEE, doi:10.1109/TRANSDUCERS.2015.7181396, 21–25 June 2015a.

Zhao, C., Wood, G. S., Xie, J., Chang, H., Pu, S. H., and Kraft, M.: A force sensor based on three weakly coupled resonators with ultrahigh sensitivity, Sensor. Actuat. A-Phys., 232, 151–162, doi:10.1016/j.sna.2015.05.011, 2015b.

Zhao, C., Wood, G., Xie, J., Chang, H., Pu, S., and Kraft, M.: A Three Degree-of-Freedom Weakly Coupled Resonator Sensor With Enhanced Stiffness Sensitivity, J. Microelectromech. S., 25, 38–51, doi:10.1109/JMEMS.2015.2490204, 2016.